INTERNATIONAL JOURNAL FOR NUMERICAL METHODS IN FLUIDS
Int. J. Numer. Meth. Fluids 2010; **62**:945–962
Published online 27 March 2009 in Wiley InterScience (www.interscience.wiley.com). DOI: 10.1002/fld.2050

An accurate gradient and Hessian reconstruction method for cell-centered finite volume discretizations on general unstructured grids

Lee J. Betchen*,† and Anthony G. Straatman

Department of Mechanical and Materials Engineering, The University of Western Ontario, London, Ont., Canada N6A 5B9

SUMMARY

In this paper, a novel reconstruction of the gradient and Hessian tensors on an arbitrary unstructured grid, developed for implementation in a cell-centered finite volume framework, is presented. The reconstruction, based on the application of Gauss' theorem, provides a fully second-order accurate estimate of the gradient, along with a first-order estimate of the Hessian tensor. The reconstruction is implemented through the construction of coefficient matrices for the gradient components and independent components of the Hessian tensor, resulting in a linear system for the gradient and Hessian fields, which may be solved to an arbitrary precision by employing one of the many methods available for the efficient inversion of large sparse matrices. Numerical experiments are conducted to demonstrate the accuracy, robustness, and computational efficiency of the reconstruction by comparison with other common methods. Copyright © 2009 John Wiley & Sons, Ltd.

Received 12 November 2008; Revised 17 February 2009; Accepted 19 February 2009

KEY WORDS: gradient reconstruction; Hessian tensor; finite volume discretization; unstructured grids

1. INTRODUCTION

In recent years, there has been a great deal of effort expended in the development of methodologies to conduct efficient and accurate computational fluid dynamics simulations, based on a finite volume formulation, on general unstructured grids (see, for example, [1–6]). The finite volume method is attractive for engineering purposes due to its simplicity, and to the fact that it ensures satisfaction of the integral forms of the conservation laws over the entire domain. However, finite volume methods do not possess the natural tools for gradient reconstruction and interpolation

*Correspondence to: Lee J. Betchen, Department of Mechanical and Materials Engineering, The University of Western Ontario, London, Ont., Canada N6A 5B9.
†E-mail: ljbetche@uwo.ca

Contract/grant sponsor: Natural Sciences and Engineering Research Council of Canada (NSERC)

on unstructured grids, which are offered by alterative methodologies such as the finite element method. Then, in order to employ a cell-centered finite volume discretization on the general, unstructured grids that are necessary for the solution of fluid flow and heat transfer problems on geometrically complex domains, it is necessary to develop accurate and efficient methods for the reconstruction of the gradient fields. Additionally, in order to evaluate the diffusive fluxes based on knowledge of the cell-centered gradients, the Hessian tensors of the dependent variables are required to interpolate the gradients to the cell faces with second-order accuracy [3].

Previous investigators have proposed a variety of methods for gradient reconstruction on unstructured finite volume grids. Barth [1] suggests two gradient reconstructions, based on either a weighted least-squares fit to the cell-centered solution fields, or an approach following from Gauss' theorem. Frink [2] and Frink and Pirzadeh [4] circumvent the need for the explicit estimation of gradient values at the cell centers by employing for the convective fluxes a solution reconstruction based on the invariant properties of tetrahedra; the diffusive fluxes are discretized by employing either a Gauss-type gradient reconstruction over volumes centered at the cell vertices [2], or a linear reconstruction over the face [4]. This approach is attractive for its simplicity and computational efficiency; however, it requires interpolation, typically based on a Laplacian-weighted averaging, of the dependent variables to the cell vertices, and is applicable only to tetrahedral grids. More recently, Baserinia and Stubley [7] have proposed an improved, unweighted least-squares reconstruction in which the gradients of the solution field are evaluated to second-order accuracy. This reconstruction also provides a first-order estimate of the Hessian tensor, and is implemented as a two-pass iterative scheme, with the second-order correction to the gradient field calculated at each iteration based on the Hessian tensor from the previous step. Karimian and Straatman [6] have suggested an iterative gradient reconstruction based on Gauss' theorem, which provides at least first-order accuracy, though the calculation of the Hessian tensor is not addressed.

The aim of the present work is to develop a gradient reconstruction that provides a fully second-order accurate estimate of the values of the gradient field, as well as a first-order accurate estimate of the Hessian tensor field, at the cell-centered nodes of a general unstructured grid consisting of arbitrary polyhedral volumes. Though methods based on the least-squares approach are typically favored for obtaining greater than first-order accuracy in gradient reconstruction, due to the relative simplicity of the formulation [8], an approach based on Gauss' theorem is employed in the present work. This approach was chosen to ensure a discretization which is robust with respect to grid quality, following from the recent investigation of Mavriplis [9], in which it was observed that even with the typical inverse-distance weighting, least-squares reconstructions tend to produce rather inaccurate estimates for the cell-centered gradients in the vicinity of highly skewed volumes on tetrahedral grids. The present reconstruction is developed in such a manner as to remain consistent with the general formulation of second-order cell-centered finite volume methods, in which quantities of interest are typically evaluated at the cell and face centroids, without introducing additional quadrature points. Additionally, a novel method is adopted in this work for the implementation of the gradient reconstruction. As shall be observed in the numerical experiments considered in the present work, the simple iterative approaches employed by previous investigators to solve the linear system resulting from the gradient and Hessian reconstruction, often exhibit poor convergence properties on general unstructured grids. Then, in the present work, the reconstruction at a given cell-centered node is expressed in terms of coefficient matrices for the values of the gradient and Hessian components at the node and its face neighbors, which may be assembled and solved using one of the many computationally efficient methods available for inverting a large sparse matrix.

DOI: 10.1002/fld

The gradient and Hessian reconstruction method described above is presented in this work in a systematic manner. First, the derivation of the discrete approximations to the cell-centered gradient and Hessian components is presented in detail. Then, the formulation of the reconstruction in terms of coefficient matrices is developed. Next, the treatment of the gradients at boundary nodes, required to close the system of equations, is detailed. Finally, numerical experiments are presented, which serve to demonstrate the accuracy, robustness, and computational efficiency of the present method by comparison with the second-order least-squares reconstruction of Baserinia and Stubley [7] and the first-order Gauss-type reconstruction of Karimian and Straatman [6].

2. GRADIENT AND HESSIAN RECONSTRUCTION

In developing the present reconstruction, we will consider the case of a general dependent variable $\phi(\mathbf{x}, t)$ whose values are known at the cell-centered nodes of an unstructured grid consisting of cells that are arbitrary polyhedra in three dimensions. Additionally, we will presume that the boundaries of the domain have been treated in a manner consistent with the fundamental finite volume approach of Patankar [10]; that is, at the centroid of each cell face coinciding with a boundary of the domain under consideration, we define a boundary node, denoted as bnd in the representative grid illustrated in Figure 1. In the present work, the value of ϕ is taken to be known at each boundary node, consistent with the formulation of Patankar [10], in which the boundary conditions for ϕ are discretized in a manner such that an appropriate estimate for the value ϕ_{bnd} is obtained. Under these conditions, no special treatment is required for the calculation of the gradient and Hessian components at cells possessing neighbors belonging to the set of boundary nodes, so long as second-order accurate estimates of the gradient vectors at the boundary nodes are formed and absorbed into coefficient matrices of their interior neighbors; this is necessary in order to close the set of equations for the Hessian reconstruction, and a suggested treatment of the gradients at boundary nodes will be given in a subsequent section of the present work. Then, if ϕ and its first partial derivatives are continuous over the volume Ω_P surrounding any interior cell-centered node P, from Gauss' theorem it is known that

$$\int_{\Omega_P} \nabla\phi \, \mathrm{d}V = \int_{\partial\Omega_P} \phi \hat{\mathbf{n}} \, \mathrm{d}S \tag{1}$$

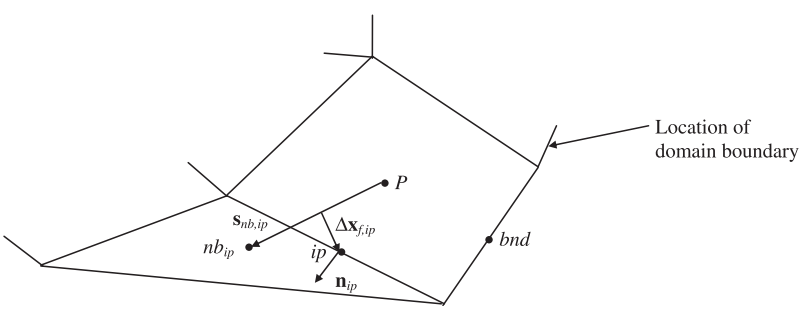

Figure 1. Representative portion of a general, unstructured, two-dimensional grid.

DOI: 10.1002/fld

where $\hat{\mathbf{n}}$ is the outward unit normal to the bounding surface $\partial\Omega_P$. Referring to the illustration of Figure 1, the surface integral of Equation (1) may be written as the sum of the integrals over the polygonal faces $\partial\Omega_{ip}$, whose union is $\partial\Omega_P$. Expanding $\nabla\phi$ in a Taylor series about the node P, located at the centroid $\mathbf{x}_P$ of the volume Ω_P, and similarly employing Taylor series for ϕ expanded about the centroid ip of each face, Equation (1) becomes

$$\int_{\Omega_P}(\nabla\phi|_P+\nabla\nabla\phi|_P\cdot(\mathbf{x}-\mathbf{x}_P)+O(\delta^2))\,\mathrm{d}V$$
$$=\sum_{ip}\int_{\partial\Omega_{ip}}\left(\phi_{ip}+\nabla\phi|_{ip}\cdot(\mathbf{x}-\mathbf{x}_{ip})+\frac{1}{2}(\mathbf{x}-\mathbf{x}_{ip})\cdot\nabla\nabla\phi|_{ip}\cdot(\mathbf{x}-\mathbf{x}_{ip})+O(\delta^3)\right)\hat{\mathbf{n}}\,\mathrm{d}S \qquad (2)$$

where δ is the characteristic grid spacing and $ip=1,2,\ldots,N_F$ for a volume with N_F faces. Noting that the planar faces of a polyhedral volume possess a constant normal $\hat{\mathbf{n}}=\hat{\mathbf{n}}_{ip}$, and employing the definition of a centroid, Equation (2) simplifies as:

$$\nabla\phi|_P+O(\delta^2)$$
$$=\frac{1}{\Omega_P}\sum_{ip}[\phi_{ip}+O(\delta^3)]\partial\Omega_{ip}\hat{\mathbf{n}}_{ip}+\frac{1}{2\Omega_P}\sum_{ip}\nabla\nabla\phi|_{ip}:\int_{\partial\Omega_{ip}}(\mathbf{x}-\mathbf{x}_{ip})(\mathbf{x}-\mathbf{x}_{ip})\hat{\mathbf{n}}\,\mathrm{d}S \qquad (3)$$

It is crucial at this juncture to note that $\partial\Omega_{ip}/\Omega_P$ is of the order of δ^{-1}. Thus, the second summation on the right side of Equation (3), which depends on the values of the Hessian tensor at the face centroids, will be of the order of δ and must in general be retained to ensure second-order accuracy. Alternatively, a second-order accurate formulation in which the Hessian tensor does not explicitly appear could be derived by taking additional quadrature points on each face in evaluating the surface integral of Equation (1); however, this approach is somewhat cumbersome for arbitrary grids, and, as mentioned above, such an approach is inconsistent with the general formulation of second-order finite volume methods. Then, as the Hessian is generally required in any event for the interpolation of gradients, in the present work we adopt the strategy of explicitly retaining the second summation on the right side of Equation (3). Noting that any first-order estimate of the Hessian tensor at the face centroids is sufficient to maintain accuracy, this summation may approximated in terms of the Hessian tensor evaluated at the cell center:

$$\sum_{ip}\nabla\nabla\phi|_{ip}:\int_{\partial\Omega_{ip}}(\mathbf{x}-\mathbf{x}_{ip})(\mathbf{x}-\mathbf{x}_{ip})\hat{\mathbf{n}}\,\mathrm{d}S=[\nabla\nabla\phi|_P+O(\delta)]:\sum_{ip}\int_{\partial\Omega_{ip}}(\mathbf{x}-\mathbf{x}_{ip})(\mathbf{x}-\mathbf{x}_{ip})\hat{\mathbf{n}}\,\mathrm{d}S \qquad (4)$$

Expanding the quadratic term in the integral on the right side of Equation (4) and simplifying:

$$\sum_{ip}\nabla\nabla\phi|_{ip}:\int_{\partial\Omega_{ip}}(\mathbf{x}-\mathbf{x}_{ip})(\mathbf{x}-\mathbf{x}_{ip})\hat{\mathbf{n}}\,\mathrm{d}S$$
$$=\nabla\nabla\phi|_P:\left(\int_{\partial\Omega_P}\mathbf{x}\mathbf{x}\hat{\mathbf{n}}\,\mathrm{d}S-\sum_{ip}\mathbf{x}_{ip}\mathbf{x}_{ip}\hat{\mathbf{n}}_{ip}\partial\Omega_{ip}\right)+O(\delta^5) \qquad (5)$$

DOI: 10.1002/fld

The remaining integral on the right side of Equation (5) may be evaluated simply by employing Gauss' theorem; this yields the form:

$$\sum_{ip} \nabla\nabla\phi|_{ip} : \int_{\partial\Omega_{ip}} (\mathbf{x}-\mathbf{x}_{ip})(\mathbf{x}-\mathbf{x}_{ip})\hat{\mathbf{n}}\,\mathrm{d}S$$
$$= 2\Omega_P \nabla\nabla\phi|_P \cdot \mathbf{x}_P - \nabla\nabla\phi|_P : \sum_{ip} \mathbf{x}_{ip}\mathbf{x}_{ip}\hat{\mathbf{n}}_{ip}\partial\Omega_{ip} + O(\delta^5) \tag{6}$$

Substituting Equation (6) into Equation (3) and collecting error terms, the final estimate to the gradient at the cell-centered node P is given as:

$$\nabla\phi|_P = \frac{1}{\Omega_P}\sum_{ip}\left[\phi_{ip} - \frac{1}{2}\nabla\nabla\phi|_P : \mathbf{x}_{ip}\mathbf{x}_{ip}\right]\partial\Omega_{ip}\hat{\mathbf{n}}_{ip} + \nabla\nabla\phi|_P \cdot \mathbf{x}_P + O(\delta^2) \tag{7}$$

It remains to develop a suitable approximation for the values of ϕ at the face-centered integration points based on knowledge of the cell-centered quantities. In order to maintain the second-order accuracy of the approximation given in Equation (7), the integration point values must be replaced with third-order accurate estimates. Referring to the geometry of Figure 1, a suitable estimate may be found, following the approach of Karimian and Straatman [6], by first interpolating the values of ϕ, $\nabla\phi$, and $\nabla\nabla\phi$ and to some point lying a fraction f_{ip} of the distance along the vector $\mathbf{s}_{nb,ip}$ connecting node P to its neighbor, then extrapolating from this point to the integration point. Suitable estimates for the value of ϕ at the points $\mathbf{x}_P + f_{ip}\mathbf{s}_{nb,ip}$ and $\mathbf{x}_{ip}$ may be derived from a straightforward Taylor series analysis and are given, respectively, as:

$$\begin{aligned}\phi_{f,ip} &= (1-f_{ip})\phi_P + f_{ip}\phi_{nb,ip} - \tfrac{1}{2}f_{ip}(1-f_{ip})\nabla\nabla\phi|_{f,ip} : \mathbf{s}_{nb,ip}\mathbf{s}_{nb,ip} + O(\delta^3)\\ \phi_{ip} &= \phi_{f,ip} + \nabla\phi|_{f,ip}\cdot\Delta\mathbf{x}_{f,ip} + \tfrac{1}{2}\nabla\nabla\phi|_{f,ip} : \Delta\mathbf{x}_{f,ip}\Delta\mathbf{x}_{f,ip} + O(\delta^3)\end{aligned} \tag{8}$$

In order to maintain the accuracy of the estimates of Equations (8), it is only necessary to develop second-order and first-order estimates, respectively, of the values of the gradient and the Hessian tensor at the point $\mathbf{x}_P + f_{ip}\mathbf{s}_{nb,ip}$; however, it is more reasonable in this instance to employ the usual second-order inverse-distance interpolation for both quantities, in order to obtain the same estimate for ϕ_{ip} at both the node P and its neighbor. Then, inserting these estimates in Equations (8) and combining, it is found that:

$$\begin{aligned}\phi_{ip} = {} & (1-f_{ip})\phi_P + f_{ip}\phi_{nb,ip} + \Delta\mathbf{x}_{f,ip}\cdot\lfloor(1-f_{ip})\nabla\phi|_P + f_{ip}\nabla\phi|_{nb,ip}\rfloor\\ & + \tfrac{1}{2}[\Delta\mathbf{x}_{f,ip}\Delta\mathbf{x}_{f,ip} - f_{ip}(1-f_{ip})\mathbf{s}_{nb,ip}\mathbf{s}_{nb,ip}] : [(1-f_{ip})\nabla\nabla\phi|_P + f_{ip}\nabla\nabla\phi|_{nb,ip}]\\ & + O(\delta^3)\end{aligned} \tag{9}$$

Karimian and Straatman [6] employ the weight $f_{ip} = 0.5$; however, in order to improve the condition of the linear system, an alternative choice employed in the present work is to take f_{ip} such that the vector $\Delta\mathbf{x}_{f,ip} = \mathbf{x}_{ip} - (\mathbf{x}_P + f_{ip}\mathbf{s}_{nb,ip})$ is perpendicular to $\mathbf{s}_{nb,ip}$, yielding:

$$f_{ip} = \frac{1}{|\mathbf{s}_{nb,ip}|^2}(\mathbf{x}_{ip} - \mathbf{x}_P)\cdot\mathbf{s}_{nb,ip} \tag{10}$$

For an arbitrarily directed gradient field, this choice of f_{ip} will tend to minimize the size of the correction term. Note also that if f_{ip} is specified as in Equation (10), the integration point value

DOI: 10.1002/fld

given by Equation (9) will reduce, as desired, to the value of the boundary neighbor for faces coinciding with the domain boundaries.

It is evident that Equations (9) and (10) provide the needed estimate of ϕ_{ip} in terms of the nodal values, and may be substituted in Equation (7) to provide a fully second-order accurate reconstruction of the gradient of ϕ at the cell-centered node P in terms of the known nodal values of ϕ, and the unknown values of the Hessian tensor at node P and its neighbors, and the gradient vector evaluated at the neighbors of node P. Then, all that is required to complete the linear system representing the gradient and Hessian reconstruction is the derivation of a suitable estimate to the values of the Hessian tensor at the cell centroids. As only a first-order accurate estimate of the Hessian is required to maintain a second-order accuracy in both the gradient reconstruction and the interpolation of cell-centered gradient values to the integration points, the components of the Hessian tensor may be estimated by applying simplified forms of Equations (7) and (9), with the Hessian-based correction terms omitted, to the gradient components $\partial\phi/\partial x_i$, yielding:

$$\begin{aligned}\nabla(\partial\phi/\partial x_i)|_P &= \frac{1}{\Omega_P}\sum_{ip}(\partial\phi/\partial x_i)_{ip}\partial\Omega_{ip}\hat{\mathbf{n}}_{ip}+O(\delta)\\ (\partial\phi/\partial x_i)_{ip} &= (1-f_{ip})(\partial\phi/\partial x_i)_P+f_{ip}(\partial\phi/\partial x_i)_{nb,ip}\\ &\quad +\Delta\mathbf{x}_{f,ip}\cdot[(1-f_{ip})\nabla(\partial\phi/\partial x_i)|_P+f_{ip}\nabla(\partial\phi/\partial x_i)|_{nb,ip}]+O(\delta^2)\end{aligned} \tag{11}$$

Then, Equation (7) and the first of the Equations (11) comprise the linear system representing the gradient and Hessian reconstruction, with the required interpolations being given by Equations (9) and (10) and the second of Equations (11).

3. COEFFICIENT MATRIX FORMULATION

Substituting Equation (9) into Equation (7), a linear system for the gradient at the cell-centered node P may be written in the form

$$\mathbf{A}_P\cdot\nabla\phi|_P=\sum_{ip}\mathbf{A}_{nb,ip}\cdot\nabla\phi|_{nb,ip}+\boldsymbol{\beta}_P+\mathbf{b}_P \tag{12}$$

where:

$$\begin{aligned}\mathbf{A}_P &= \mathbf{I}-\frac{1}{\Omega_P}\sum_{ip}[\partial\Omega_{ip}(1-f_{ip})\hat{\mathbf{n}}_{ip}\Delta\mathbf{x}_{f,ip}]\\ \mathbf{A}_{nb,ip} &= \frac{1}{\Omega_P}[\partial\Omega_{ip}f_{ip}\hat{\mathbf{n}}_{ip}\Delta\mathbf{x}_{f,ip}]\\ \boldsymbol{\beta}_P &= \nabla\nabla\phi|_P\cdot\mathbf{x}_P+\frac{1}{2\Omega_P}\sum_{ip}[\partial\Omega_{ip}([\Delta\mathbf{x}_{f,ip}\Delta\mathbf{x}_{f,ip}\\ &\quad -f_{ip}(1-f_{ip})\mathbf{s}_{nb,ip}\mathbf{s}_{nb,ip}]:[(1-f_{ip})\nabla\nabla\phi|_P+f_{ip}\nabla\nabla\phi|_{nb,ip}]-\nabla\nabla\phi|_P:\mathbf{x}_{ip}\mathbf{x}_{ip})\hat{\mathbf{n}}_{ip}]\\ \mathbf{b}_P &= \frac{1}{\Omega_P}\sum_{ip}[\partial\Omega_{ip}([1-f_{ip}]\phi_P+f_{ip}\phi_{nb,ip})\hat{\mathbf{n}}_{ip}]\end{aligned} \tag{13}$$

DOI: 10.1002/fld

The term $\boldsymbol{\beta}_P$ in Equations (12) and (13) contains all of the Hessian-based corrections required to ensure second-order accuracy in the reconstruction. The reconstruction of a vectorized form of the Hessian, obtained by writing Equations (11) for $i \in \{1, 2, 3\}$, may be cast in a similar form as

$$\mathbf{A}'_P \cdot \begin{bmatrix} \nabla(\partial\phi/\partial x_1)|_P \\ \nabla(\partial\phi/\partial x_2)|_P \\ \nabla(\partial\phi/\partial x_3)|_P \end{bmatrix} = \sum_{ip} \mathbf{A}'_{nb,ip} \cdot \begin{bmatrix} \nabla(\partial\phi/\partial x_1)|_{nb,ip} \\ \nabla(\partial\phi/\partial x_2)|_{nb,ip} \\ \nabla(\partial\phi/\partial x_3)|_{nb,ip} \end{bmatrix} + \mathbf{b}'_P \tag{14}$$

where:

$$\begin{aligned} \mathbf{A}'_P &= \begin{bmatrix} \mathbf{A}_P & \mathbf{O} & \mathbf{O} \\ \mathbf{O} & \mathbf{A}_P & \mathbf{O} \\ \mathbf{O} & \mathbf{O} & \mathbf{A}_P \end{bmatrix} \\ \mathbf{A}'_{nb,ip} &= \begin{bmatrix} \mathbf{A}_{nb,ip} & \mathbf{O} & \mathbf{O} \\ \mathbf{O} & \mathbf{A}_{nb,ip} & \mathbf{O} \\ \mathbf{O} & \mathbf{O} & \mathbf{A}_{nb,ip} \end{bmatrix} \\ \mathbf{b}'_P &= \begin{bmatrix} \mathbf{b}'_{P,1} \\ \mathbf{b}'_{P,2} \\ \mathbf{b}'_{P,3} \end{bmatrix} \\ \mathbf{b}'_{P,i} &= \frac{1}{\Omega_P} \sum_{ip} [\partial\Omega_{ip}([1 - f_{ip}](\partial\phi/\partial x_i)_P + f_{ip}(\partial\phi/\partial x_i)_{nb,ip})\hat{\mathbf{n}}_{ip}] \end{aligned} \tag{15}$$

Note that, for continuous functions ϕ with continuous first and second partial derivatives, the Hessian is symmetric, so that in three dimensions only six of the nine components of each unknown vector in Equation (14) are independent. Then, in the interest of both computational efficiency and reasonableness of the solution, we will solve only for these independent components. Taking the vector $\mathbf{h}(\phi)$ to contain the independent components of the Hessian, a matrix $\mathbf{C}$ may be defined such that:

$$\begin{bmatrix} \nabla(\partial\phi/\partial x_1) \\ \nabla(\partial\phi/\partial x_2) \\ \nabla(\partial\phi/\partial x_3) \end{bmatrix} = \mathbf{C} \cdot \mathbf{h}(\phi) \tag{16}$$

Substituting Equation (16) into Equation (14) yields an over-determined system for $\mathbf{h}(\phi)|_P$, which may be reduced using a least-squares procedure to the fully determined system:

$$[(\mathbf{A}'_P \cdot \mathbf{C})^{\mathrm{T}} \cdot (\mathbf{A}'_P \cdot \mathbf{C})] \cdot \mathbf{h}(\phi)|_P = \sum_{ip} [(\mathbf{A}'_P \cdot \mathbf{C})^{\mathrm{T}} \cdot (\mathbf{A}'_{nb,ip} \cdot \mathbf{C})] \cdot \mathbf{h}(\phi)|_{nb,ip} + (\mathbf{A}'_P \cdot \mathbf{C})^{\mathrm{T}} \cdot \mathbf{b}'_P \tag{17}$$

In the gradient reconstruction of Equation (12), the values of the Hessian tensor at the P node and its neighbors appear in the term $\boldsymbol{\beta}_P$; similarly, the values of the gradient vector over the same stencil appear in the Hessian reconstruction of Equation (17) through the term $\mathbf{b}'_P$. Then, in order

DOI: 10.1002/fld

to allow the solution of the reconstructions by a general numerical method for inverting a sparse linear system, the gradient and Hessian reconstructions at node P must be combined into a single system of the form

$$\tilde{\mathbf{A}}_P \cdot \mathbf{G}(\phi)|_P = \sum_{ip} \tilde{\mathbf{A}}_{nb,ip} \cdot \mathbf{G}(\phi)|_{nb,ip} + \tilde{\mathbf{b}}_P \tag{18}$$

where the unknown vector $\mathbf{G}(\phi)$ is given as:

$$\mathbf{G}(\phi) = \begin{bmatrix} \nabla\phi \\ \mathbf{h}(\phi) \end{bmatrix} \tag{19}$$

The values of the components of the unknown vector $\tilde{\mathbf{b}}_P$ in Equation (18) must be independent of the gradient and Hessian fields. Then, it may be shown from Equations (12)–(17) that

$$\begin{aligned} \tilde{\mathbf{A}}_P &= \begin{bmatrix} \mathbf{A}_P & -\mathbf{B}_P \\ -(\mathbf{A}'_P \cdot \mathbf{C})^{\mathrm{T}} \cdot \mathbf{B}'_P & (\mathbf{A}'_P \cdot \mathbf{C})^{\mathrm{T}} \cdot (\mathbf{A}'_P \cdot \mathbf{C}) \end{bmatrix} \\ \tilde{\mathbf{A}}_{nb,ip} &= \begin{bmatrix} \mathbf{A}_{nb,ip} & \mathbf{B}_{nb,ip} \\ (\mathbf{A}'_P \cdot \mathbf{C})^{\mathrm{T}} \cdot \mathbf{B}'_{nb,ip} & (\mathbf{A}'_P \cdot \mathbf{C})^{\mathrm{T}} \cdot (\mathbf{A}'_{nb,ip} \cdot \mathbf{C}) \end{bmatrix} \\ \tilde{\mathbf{b}}_P &= \begin{bmatrix} \mathbf{b}_P \\ \mathbf{O} \end{bmatrix} \end{aligned} \tag{20}$$

where the matrices $\mathbf{B}_P$ and $\mathbf{B}_{nb,ip}$ are determined by writing the vector $\boldsymbol{\beta}_P$ of Equation (13) in the form

$$\boldsymbol{\beta}_P = \mathbf{B}_P \cdot \mathbf{h}(\phi)|_P + \sum_{ip} \mathbf{B}_{nb,ip} \cdot \mathbf{h}(\phi)|_{nb,ip} \tag{21}$$

while $\mathbf{B}'_P$ and $\mathbf{B}'_{nb,ip}$ are similarly determined from $\mathbf{b}'_P$ according to:

$$\mathbf{b}'_P = \mathbf{B}'_P \cdot \mathbf{h}(\phi)|_P + \sum_{ip} \mathbf{B}'_{nb,ip} \cdot \mathbf{h}(\phi)|_{nb,ip} \tag{22}$$

Then, casting the third of Equations (13) in the form of Equation (21), it is found that

$$\begin{aligned} (\mathbf{B}_P)_{ij} &= (\mathbf{x}_P)_k P_{ikj} + \frac{P_{kmj}}{2\Omega_P} \sum_{ip} ([1 - f_{ip}][(\Delta\mathbf{x}_{f,ip})_k (\Delta\mathbf{x}_{f,ip})_m \\ &\quad - f_{ip}(1 - f_{ip})(\mathbf{s}_{nb,ip})_k (\mathbf{s}_{nb,ip})_m] - [\mathbf{x}_{ip}]_k [\mathbf{x}_{ip}]_m) \partial\Omega_{ip} (\hat{\mathbf{n}}_{ip})_i \\ (\mathbf{B}_{nb,ip})_{ij} &= \frac{\partial\Omega_{ip} f_{ip} (\hat{\mathbf{n}}_{ip})_i P_{kmj}}{2\Omega_P} [(\Delta\mathbf{x}_{f,ip})_k (\Delta\mathbf{x}_{f,ip})_m - f_{ip}(1 - f_{ip})(\mathbf{s}_{nb,ip})_k (\mathbf{s}_{nb,ip})_m] \end{aligned} \tag{23}$$

where $i, j, k, m \in \{1, 2, 3\}$, with summation implied over k and m, and where the third-order tensor P_{ijk} is defined according to the relation:

$$(\nabla\nabla\phi)_{ij} = P_{ijk} [\mathbf{h}(\phi)]_k \tag{24}$$

DOI: 10.1002/fld

From the third and fourth of Equations (15), the matrices $\mathbf{B}'_P$ and $\mathbf{B}'_{nb,ip}$ are obtained as:

$$\mathbf{B}'_P = \begin{bmatrix} \mathbf{d}_P & \mathbf{O} & \mathbf{O} \\ \mathbf{O} & \mathbf{d}_P & \mathbf{O} \\ \mathbf{O} & \mathbf{O} & \mathbf{d}_P \end{bmatrix}$$

$$\mathbf{B}'_{nb,ip} = \begin{bmatrix} \mathbf{d}_{nb,ip} & \mathbf{O} & \mathbf{O} \\ \mathbf{O} & \mathbf{d}_{nb,ip} & \mathbf{O} \\ \mathbf{O} & \mathbf{O} & \mathbf{d}_{nb,ip} \end{bmatrix} \tag{25}$$

$$\mathbf{d}_P = \frac{1}{\Omega_P} \sum_{ip} \partial\Omega_{ip} \hat{\mathbf{n}}_{ip} (1 - f_{ip})$$

$$\mathbf{d}_{nb,ip} = \frac{1}{\Omega_P} \partial\Omega_{ip} \hat{\mathbf{n}}_{ip} f_{ip}$$

With the definitions of Equations (24) and (25), the system represented by Equations (18)–(20) is now complete; assembling this system over all cells and absorbing appropriate conditions for the gradient vectors at the boundary nodes, as addressed in the next section of the present work, yields a sparse, block-structured global coefficient matrix which may be inverted to obtain the reconstructed values of the cell-centered gradients and Hessian tensors. While this system appears rather complex, it should be noted that $\tilde{\mathbf{A}}_P$ and $\tilde{\mathbf{A}}_{nb,ip}$ depend only on the grid geometry, so that, for a fixed grid, the coefficient matrices need only be evaluated once. For the numerical experiments considered in this work, the linear system represented by Equation (18) was solved using an under-relaxed block-Jacobi method. Under this method, $\tilde{\mathbf{A}}_P^{-1}$ and $\tilde{\mathbf{A}}_{nb,ip}$ may be constructed and stored once; then, for each reconstruction to be performed, the $\tilde{\mathbf{b}}_P$ vectors are calculated, and the solution proceeds from iteration n to $n+1$ according to

$$\mathbf{G}(\phi)|_P^{n+1} = \alpha \mathbf{G}(\phi)|_P^n + (1-\alpha) \tilde{\mathbf{A}}_P^{-1} \cdot \left(\sum_{ip} \tilde{\mathbf{A}}_{nb,ip} \cdot \mathbf{G}(\phi)|_{nb,ip}^n + \tilde{\mathbf{b}}_P \right) \tag{26}$$

for some relaxation parameter $\alpha \in [0, 1)$; in general, for an arbitrary grid, $\alpha > 0$ will be required to ensure convergence. This method of solution is simple to implement, requires little memory overhead, and is reasonably robust and computationally efficient, however, with the reconstruction formulated in terms of the coefficient matrices given in Equations (20), any desirable method may be employed for the inversion of the global coefficient matrix.

4. BOUNDARY TREATMENT

Consider the formulation of the system of Equations (18)–(20) for a volume neighbored by one or more boundary nodes, such as the volume centered about the node P illustrated in Figure 1.

DOI: 10.1002/fld

From the forgoing derivation, it may be shown that the neighbor coefficient matrix given by the second of Equations (20) reduces at a boundary neighbor to the form

$$\tilde{\mathbf{A}}_{nb,ip} = \begin{bmatrix} \mathbf{O} & \mathbf{O} \\ (\mathbf{A}'_P \cdot \mathbf{C})^{\mathrm{T}} \cdot \mathbf{B}'_{nb,ip} & \mathbf{O} \end{bmatrix} \tag{27}$$

since $f_{ip} = 1$ and $\Delta\mathbf{x}_{f,ip} = 0$ for integration points ip associated with boundary neighbors. As noted above, it is evident from the form of Equation (27) that, in order to obtain a closed set of equations for the reconstruction, the specification of an appropriate boundary condition for the gradient field is necessary. While it is possible to develop a reconstruction for the gradients at the boundary nodes, this approach is somewhat cumbersome, particularly if it is desired to obtain second-order accurate approximations to the gradients at the boundary nodes, as is necessary to maintain first-order accuracy in the Hessian reconstruction. Instead, we propose, and implement in the present work, the straightforward extrapolated condition

$$\nabla\phi|_{\mathrm{bnd}} = \nabla\phi|_P + \overline{\nabla\nabla\phi}|_P \cdot (\mathbf{x}_{\mathrm{bnd}} - \mathbf{x}_P) + O(\delta^2) \tag{28}$$

where $\overline{\nabla\nabla\phi}|_P$ is any first-order accurate approximation of the Hessian at node P. It is important to note that simply choosing $\overline{\nabla\nabla\phi}|_P = \nabla\nabla\phi|_P$ in the implementation of Equation (28) may in some instances leave the system of equations underdetermined. As a trivial illustration, consider the case of a two-dimensional grid that has simply been extruded in the out-of-plane direction x_3, with only a single plane of cells normal to that direction. Clearly, in this case the value of $\partial^2\phi/\partial x_3^2|_P$ at each cell would be arbitrary under the condition of Equation (28) with $\overline{\nabla\nabla\phi}|_P = \nabla\nabla\phi|_P$. Then, in the present work, we approximate $\overline{\nabla\nabla\phi}|_P$ as the inverse-distance-averaged Hessian tensor averaged over the interior neighbors of P, which are not adjacent to the domain boundary; that is, if we consider IP^* to be the set of faces of P such that the associated neighbors nb_{ip}, where $ip \in IP^*$, are interior nodes that are not themselves neighbored by any boundary nodes, then:

$$\overline{\nabla\nabla\phi}|_P = \begin{bmatrix} 0, & IP^* = \emptyset \\ \dfrac{\sum_{ip\in IP^*} (\nabla\nabla\phi|_{nb,ip} / |\mathbf{s}_{nb,ip}|)}{\sum_{ip\in IP^*} |\mathbf{s}_{nb,ip}|^{-1}} & \text{otherwise} \end{bmatrix} \tag{29}$$

Clearly, the approximation of Equation (29) yields $\overline{\nabla\nabla\phi}|_P = \nabla\nabla\phi|_P + O(\delta)$ whenever IP^* is non-empty, so that the order of the reconstruction is maintained for any reasonable grid. The proposed boundary condition may easily be cast in the form

$$\nabla\phi|_{\mathrm{bnd}} = \nabla\phi|_P + \sum_{ip\in IP^*} \overline{\mathbf{A}_{nb,ip}} \cdot \nabla\nabla\phi|_{nb,ip} \tag{30}$$

and absorbed into the coefficient matrices for the reconstruction at node P. Note that the condition of Equations (28)–(29) is employed simply to close the set of equations for the reconstruction of the gradient and Hessian tensor fields at the interior cell-centered nodes in such a manner as to maintain the order of accuracy of the reconstruction. For a boundary on which a Robin-type condition is specified for the computational fluid dynamics problem, for example, the gradients obtained from Equations (28)–(29) will not necessarily satisfy this condition; thus, these gradient values should not be used to calculate diffusive fluxes at the boundaries without appropriate modification.

DOI: 10.1002/fld

5. NUMERICAL EXPERIMENTS

Numerical experiments have been conducted to validate the proposed methodology for the computation of the gradient reconstruction, and to compare the second-order Gauss' theorem-based approach developed above with the basic Gauss-type reconstruction proposed by Karimian and Straatman [6], and also with the second-order least-squares approach of Baserinia and Stubley [7]. Note that as Karimian and Straatman [6] did not consider the reconstruction of the Hessian tensor, the Hessian reconstruction developed above was employed in combination with the basic Gauss' theorem approach, resulting in coefficient matrices and right side vectors identical to those given in Equations (20), with the exception that the $\mathbf{B}_P$ and $\mathbf{B}_{nb,ip}$ matrices, associated with the $\boldsymbol{\beta}_P$ term of Equation (13), are neglected. In each case, the coefficient matrices appearing in Equation (18) were formed and employed to compute the cell-centered gradients and Hessian tensors for the test function

$$\phi = \frac{1}{|\mathbf{x}|} \tag{31}$$

on the domain illustrated in Figure 2, which is a three-dimensional extension of the domain considered by Baserinia and Stubley [7]. The domain was constructed with $H/D = 2$, where H is the side length of the cubic domain, and D is the diameter of the spherical void centered about the centroid of the cube. In order to perform a grid convergence study, three tetrahedral grids, each with refinement toward the spherical void, were constructed for this geometry. In particular, each grid was generated using the commercially available grid generation software, Gambit [11], employing the TGrid scheme. The mean edge length of the tetrahedra adjacent to the spherical void, the maximum mean edge length, the growth rate of successive layers of tetrahedra, and the total number of volumes are given in Table I for the each of the coarse, medium, and fine grids. Such grids are straightforward to construct with a commercial grid generator such as Gambit, requiring only the creation of the geometry and the imposition of a single fixed size function to control the refinement; such grids were thus selected as representative of the sort of grid typically employed in industrial computational fluid dynamics calculations. A section view of the medium

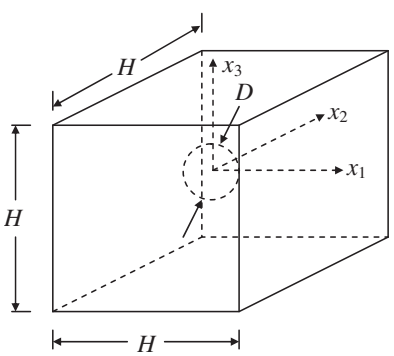

Figure 2. Geometry for validation case.

DOI: 10.1002/fld

Table I. Characterization of grids employed in the numerical experiments.

	Coarse grid	Medium grid	Fine grid
Mean edge length at $\|\mathbf{x}\|=0.5D$	$0.058D$	$0.04D$	$0.028D$
Maximum mean edge length	$0.174D$	$0.12D$	$0.084D$
Growth rate per layer of tetrahedra (%)	10	10	10
Total number of volumes N_V	89 306	186 522	369 892

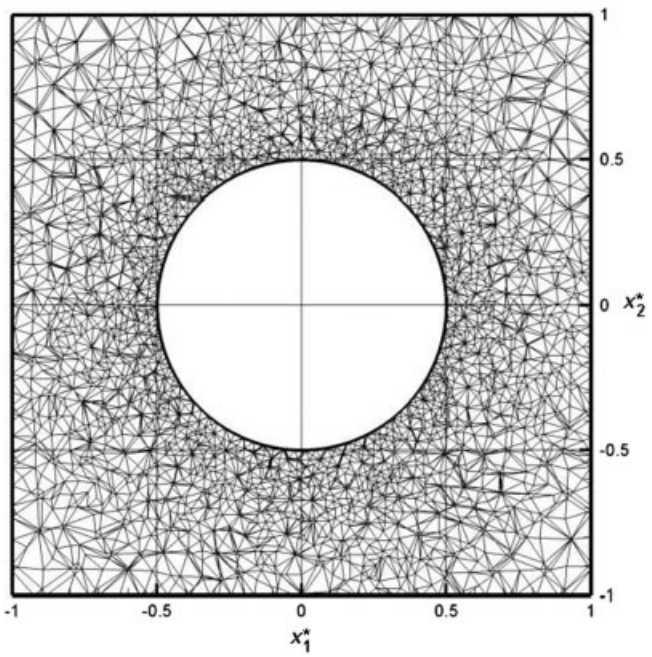

Figure 3. Section view of medium grid at $x_3^*=0$.

grid is given in Figure 3. Unless otherwise noted, the normalized residual between successive iterations of the solver was reduced below the level 10^{-4} at every volume. For convenience, the results of the present study are reported in dimensionless form, with:

$$\begin{aligned} \phi^* &= \phi D \\ x_i^* &= x_i / D \end{aligned} \tag{32}$$

In light of the symmetry of the test function and domain, it is sufficient in the following analysis to examine the reconstructions of $\partial\phi^*/\partial x_1^*$, $\partial^2\phi^*/\partial x_1^{*2}$, and $\partial^2\phi^*/\partial x_1^*\partial x_2^*$.

In order to characterize the dependence upon grid spacing of the truncation error in each of the reconstructions considered, a grid convergence study has been conducted. Following from the

DOI: 10.1002/fld

derivation presented above, we presume for some reconstructed gradient estimate $\overline{\nabla^* \phi^*}$ which the local error follows:

$$(\varepsilon_i)_P = \left| \left. \frac{\partial \phi^*}{\partial x_i^*} \right|_P - \left. \overline{\frac{\partial \phi^*}{\partial x_i^*}} \right|_P \right| = (\beta_i)_P \left(\frac{\delta}{D} \right)^{\gamma_i} \tag{33}$$

Then, taking the volume-weighted average of the local error over a grid of N_V volumes, the average error is obtained as

$$\begin{aligned} \langle \varepsilon_i \rangle &= \frac{1}{\Omega} \sum_P (\varepsilon_i)_P \Omega_P \\ &= \left(\frac{1}{\Omega} \sum_P (\beta_i)_P \Omega_P \right) \left(\frac{\delta}{D} \right)^{\gamma_i} \\ &= \langle \beta_i \rangle \left(\frac{\delta}{D} \right)^{\gamma_i} \end{aligned} \tag{34}$$

where Ω is the total volume of the domain of simulation, and $i \in \{1, 2, 3\}$ with no summation implied over i. Similarly, the average error in the Hessian component $\partial^2 \phi^* / \partial x_i^* \partial x_j^*$ may be shown to follow

$$\langle \varepsilon_{ij} \rangle = \langle \beta_{ij} \rangle \left(\frac{\delta}{D} \right)^{\gamma_{ij}} \tag{35}$$

where $i, j \in \{1, 2, 3\}$ with no summation implied over i or j. Taking the factors $\langle \beta_i \rangle$ and $\langle \beta_{ij} \rangle$, which depend on the derivatives of ϕ and on the relationship of the local grid spacing to the characteristic value δ, to be approximately constant over the grids characterized in Table I, the effective orders γ_i and γ_{ij} of the reconstructed estimates of the gradient and Hessian components may be computed by fitting the average error values obtained on the coarse, medium, and fine grids to Equations (34) and (35) using a least-squares approach. In order to fit the data obtained from the grid convergence study, it is necessary only to define an appropriate value for the characteristic grid spacing; in the present work, we use the cube root of the average cell volume, $\delta = (\Omega / N_V)^{1/3}$. Table II presents the values of γ_1, γ_{11}, and γ_{12} obtained for the reconstruction proposed in the present work, as well as the reconstructions proposed by Karimian and Straatman [6], and Baserinia and Stubley [7]. From Table II, it may be seen that for both the present approach and the second-order least-squares approach of Baserinia and Stubley, the average truncation errors in the components of the gradient field indeed vary approximately as the square of the characteristic grid spacing, with the errors in the Hessian components varying approximately linearly; in each case, the second-order least-squares approach yields a marginally higher-order estimate than the second-order Gauss' theorem approach. As expected, the basic Gauss' theorem approach of Karimian and Straatman [6] provides an approximately first-order accurate estimate of the gradient field, leading to the presence of essentially zero-order errors in the Hessian components. Such a method will not converge to the correct values for the Hessian components with additional grid refinement, and thus is not appropriate if accurate values are required for the Hessian field.

Contour plots of $\partial^2 \phi^* / \partial x_1^{*2}$ at the planes $x_2^* = 0$ and $x_3^* = 0$ for each approach, calculated on the medium grid, are given in Figure 4, while Table III reports the volume-weighted average and maximum error values for computations on the medium grid, in comparison with the analytical

DOI: 10.1002/fld

Table II. Order estimate of truncation error for each reconstruction scheme from grid refinement study.

	Basic Gauss theorem reconstruction [6]	Second-order Gauss theorem reconstruction	Second-order least squares reconstruction [7]
γ_1 $(\partial\phi^*/\partial x_1^*)$	0.860	1.832	1.928
γ_{11} $(\partial^2\phi^*/\partial x_1^{*2})$	−0.003	0.997	1.048
γ_{12} $(\partial^2\phi^*/\partial x_1^*\partial x_2^*)$	−0.033	0.981	1.147

solutions for the gradient and Hessian. The errors in the gradient components are given as a percentage of the integral-averaged value over the domain of the magnitude of the gradient vector, whereas the errors in the Hessian components are reported as a percentage of the average Frobenius norm of the Hessian tensor. Examining Figure 4, the advantage of employing a reconstruction that provides a second-order accurate estimate of the gradient field, and thus a fully first-order estimate of the Hessian tensor, becomes clear. While both second-order schemes produce smooth results over most of the domain, the basic Gauss' theorem approach yields spurious oscillations. This is also evident from an examination of the average error values given in Table III. Further to this, when the maximum residuals shown in Table III are examined, the advantage of the second-order Gauss' theorem approach derived above over the least-squares reconstruction of Baserinia and Stubley [7] becomes clear. The rather large maximum errors observed in the gradient and, especially, Hessian components for the second-order least-squares reconstruction, which are of the order of those observed in the first-order Gauss' theorem approach, are consistent with the findings of Mavriplis [9]. In his investigation, Mavriplis [9] observed that even weighted least-squares procedures fail to produce an adequate gradient reconstruction on tetrahedral grids in the vicinity of highly skewed volumes. Defining the aspect ratio of a tetrahedral volume as [11]

$$\rho = \frac{1}{3}\left(\frac{R_{\text{cir}}}{R_{\text{ins}}}\right) \tag{36}$$

where R_{cir} and R_{ins} are, respectively, the radii of the spheres circumscribing and inscribing the tetrahedron, it may be seen that the present grid, with a mean aspect ratio of 1.23, is of reasonably good quality throughout the majority of the grid; note that $\rho \geqslant 1$ for any tetrahedron, with $\rho = 1$ for an equilateral volume. However, the maximum aspect ratio observed on the present grid was 3.44; such an aspect ratio represents a substantial deviation from the ideal, equilateral cell geometry, and further suggests local grid quality as an explanation for the poor performance of the second-order least-squares approach. Indeed, the maximum error observed for the second-order least-squares reconstruction, in the Hessian component $\partial^2\phi^*/\partial x_1^*\partial x_2^*$, was found to occur in a volume one layer of tetrahedra removed from the spherical boundary, in a region where both the aspect ratios of the local cells, and the values of the Hessian components, were observed to be large. In light of the forgoing discussion, it would seem that for unstructured grids composed of arbitrary polyhedra, the second-order Gauss' theorem-based method derived in the present work generally provides a better combination of accuracy and robustness than previous reconstructions based on least squares or more simplistic Gauss' theorem approaches.

While the forgoing discussion clearly indicates the advantages of the present approach over previously proposed gradient and Hessian reconstruction methods in terms of accuracy and robustness, it is also necessary to consider the relative cost of the proposed method in terms of computational

DOI: 10.1002/fld

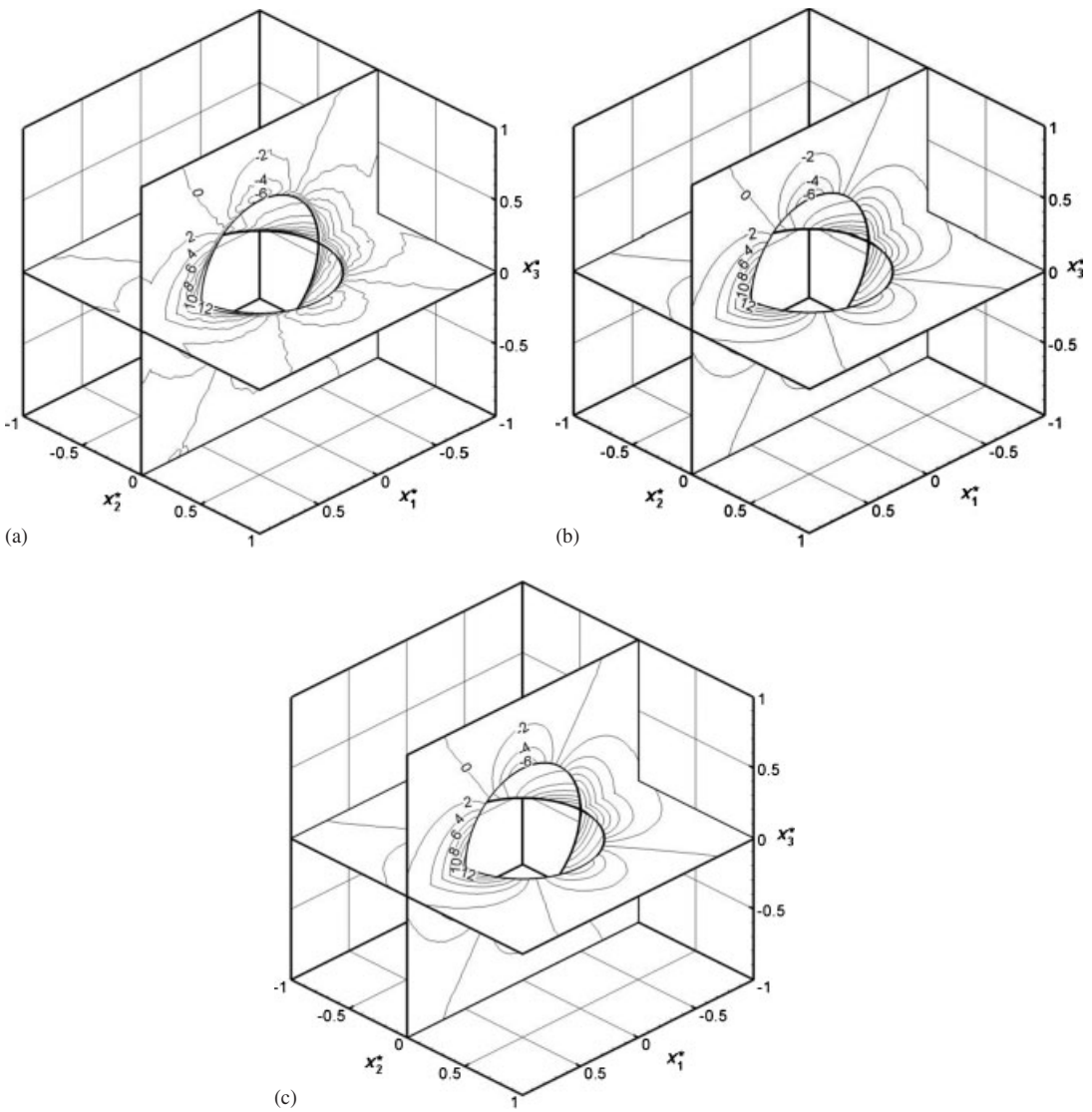

Figure 4. Contour plots of $\partial^2\phi^*/\partial x_1^{*2}$ at planes $x_2^*=0$ and $x_3^*=0$, computed on the medium grid, for (a) the basic Gauss theorem reconstruction of Karimian and Straatman [6]; (b) the present second-order Gauss theorem method; and (c) the second-order least-squares approach of Baserinia and Stubley [7].

effort. In order to demonstrate the computational efficiency of the proposed approach, the CPU time required for the solution of the present second-order Gauss' theorem-based gradient and Hessian reconstruction by the method of Equation (26) was measured and compared with the time required to obtain a converged solution, for the gradient field only, to the basic Gauss-type reconstruction of Karimian and Straatman [6]. The reconstruction of Karimian and Straatman was solved by the simple iterative solution procedure suggested in that work, with the slight modification that a

DOI: 10.1002/fld

Table III. Average and maximum percentage errors for each reconstruction scheme on medium grid.

	Basic Gauss theorem reconstruction [6] (%)	Second-order Gauss theorem reconstruction (%)	Second-order least squares reconstruction [7] (%)
Average error			
$\partial\phi^*/\partial x_1^*$	1.4	0.022	0.026
$\partial^2\phi^*/\partial x_1^{*2}$	18	1.2	1.2
$\partial^2\phi^*/\partial x_1^*\partial x_2^*$	14	0.71	0.67
Maximum error			
$\partial\phi^*/\partial x_1^*$	15	0.35	12
$\partial^2\phi^*/\partial x_1^{*2}$	360	26	380
$\partial^2\phi^*/\partial x_1^*\partial x_2^*$	280	16	430

relaxation parameter ω was introduced such that the solution proceeds from iteration n to $n+1$ according to

$$\nabla\phi|_P^{n+1} = \omega\nabla\phi|_P^n + \frac{(1-\omega)}{\Omega_P}\sum_{ip}\phi_{ip}^n\partial\Omega_{ip}\hat{\mathbf{n}}_{ip} \tag{37}$$

where the values ϕ_{ip}^n are the estimates to the values of ϕ at the integration points based on the gradient field at iteration n. In both cases, the normalized residual between successive iterations of the solver was reduced below the level 10^{-4} at every volume. For the present problem, a value of the relaxation parameter $\omega=0.4$ was required to obtain a converged solution to the reconstruction of Karimian and Straatman, whereas $\alpha=0.2$ was sufficient for the solution of the reconstruction proposed in the present work by the procedure of Equation (26). With the solution computed for each reconstruction on a single 2.2 GHz AMD Opteron processor, the CPU time required for the present gradient and Hessian reconstruction was 16.9 s, while for the reconstruction of Karimian and Straatman [6], computing only the gradient field, 192.9 s of CPU time was needed. This large difference in computational effort may be explained by considering that for the present reconstruction, convergence to the imposed criterion required 33 iterations of the block-Jacobi procedure detailed in Equation (26), while for the reconstruction of Karimian and Straatman, 1672 iterations of the solver outlined in Equation (37) were necessary to obtain a converged solution. Note that, in light of the above discussion, the time required to compute the coefficient matrices for the present reconstruction was not included in the figure given above. It is unfortunately not possible to compare the computational efficiency of the present approach to that proposed by Baserinia and Stubley [7] since, while both Gauss' theorem-based reconstructions could be converged to the required tolerance using the simple block-Jacobi solver outlined in Equation (26), the second-order least-squares reconstruction diverged for the present case under this solution procedure, as well as under the simple iterative approach suggested by Baserinia and Stubley. In order to obtain a converged solution for the least-squares approach, it is necessary to use a stabilized, pre-conditioned conjugate gradient procedure in comparison with the block-Jacobi solver of Equation (26); this solution method is rather onerous in its memory requirements on a grid of the size considered here. Clearly, when implemented in the coefficient matrix formulation and solved with any reasonably efficient method for the inversion of large sparse matrices, the second-order Gauss' theorem-based reconstruction proposed in the present work is capable of providing accurate, converged solutions

DOI: 10.1002/fld

for the gradient and Hessian tensor fields on general unstructured grids composed of arbitrary polyhedra, without requiring excessive computational effort. Furthermore, though the numerical experiments presented in this paper were conducted in a serial manner, the coefficient matrix formulation lends itself to parallelization of the gradient and Hessian reconstruction in a manner precisely similarly to that typically employed for the solution of the flow field. Such parallelization obviously would further improve performance and, in a distributed-memory environment, would allow for the use of very large grids without the memory requirements imposed by the storage of the coefficient matrices becoming too burdensome.

Finally, in order to emphasize the importance of obtaining converged results for the gradient and Hessian reconstruction, the second-order Gauss' theorem reconstruction was recalculated without residual checking; the reconstruction was simply terminated after four iterations of the solver, as suggested by Karimian and Straatman [3]. Under this stopping criterion, average errors increased greatly with an error of 22% observed for the Hessian component $\partial^2\phi^*/\partial x_1^{*2}$. Then, if accurate values for the gradient and, especially, Hessian components are desired, an adequate convergence criterion must be enforced, and as noted above, in general this is much better achieved through the use of the coefficient matrix formulation employed in the present work.

6. CONCLUSIONS

In the work presented above, a gradient reconstruction has been developed, which provides a fully second-order accurate estimate of the values of the gradient field, as well as a first-order accurate estimate of the Hessian tensor field, at the cell-centered nodes of a general unstructured grid consisting of arbitrary polyhedral volumes. The combined reconstruction, developed based on Gauss' theorem, has been expressed in terms of coefficient matrices for the values of the gradient and Hessian components at the node and its face neighbors, which may be assembled and solved using one of the many computationally efficient methods available for inverting a large sparse matrix. The results of the numerical experiments presented above suggest that the present reconstruction is generally more accurate and robust than previous reconstructions based on least squares or more simplistic Gauss' theorem approaches, and provides good computational efficiency if any reasonable method is employed to solve the linear system resulting from the reconstruction. These results also demonstrate the importance of obtaining a converged solution to the linear system representing the reconstruction, which is best accomplished by means of the coefficient matrix formulation presented herein.

NOMENCLATURE

D	diameter of spherical void (m)
f_{ip}	fraction of distance along vector $\mathbf{s}_{nb,ip}$
$\mathbf{G}(\phi)$	combined solution vector containing gradient and Hessian components
H	side length of cubic domain (m)
$\mathbf{h}(\phi)$	vector containing independent components of the Hessian tensor
$\mathbf{n}$	outward normal unit vector
N_F	number of faces of arbitrary polyhedral volume
N_V	total number of volumes

DOI: 10.1002/fld

$\mathbf{s}_{nb,ip}$	vector joining cell-centered node P to neighbor nb across face ip (m)
t	time (s)
$\mathbf{x}$	Cartesian position vector $\mathbf{x}=(x_1, x_2, x_3)$ (m)

Greek Symbols

α, ω	relaxation parameters
δ	characteristic grid spacing (m)
ε	error in reconstructed gradient or Hessian component
$\Delta\mathbf{x}_{f,ip}$	correction vector defined by $\Delta\mathbf{x}_{f,ip}=\mathbf{x}_{ip}-(\mathbf{x}_P+f_{ip}\mathbf{s}_{nb,ip})$ (m)
ϕ	general dependent variable
ρ	grid aspect ratio
Ω	spatial domain in three dimensions (m^3)
$\partial\Omega$	area bounding Ω (m^2)

Subscripts and Superscripts

ip	face-centered integration point
nb	face neighbor of node P
P	cell-centered node under consideration
*	denotes dimensionless quantity
$\langle\ \rangle$	denotes volume-weighted averaging

ACKNOWLEDGEMENTS

The authors wish to acknowledge the financial support of the Natural Sciences and Engineering Research Council of Canada (NSERC).

REFERENCES

1. Barth TJ. A 3-D upwind Euler solver for unstructured meshes. *AIAA Paper 91-1548*, 1991.
2. Frink NT. Recent progress toward a three-dimensional unstructured Navier–Stokes solver. *AIAA Paper 94-0061*, 1994.
3. Demirdzic I, Muzaferija S. Numerical method for coupled fluid flow, heat transfer, and stress analysis using unstructured moving meshes with cells of arbitrary topology. *Computer Methods in Applied Mechanics and Engineering* 1995; **125**:235–255.
4. Frink NT, Pirzadeh SZ. Tetrahedral finite-volume solutions to the Navier–Stokes equations on complex configurations. *International Journal for Numerical Methods in Fluids* 1999; **31**:175–407.
5. Basara B. Employment of the second-moment turbulence closure on arbitrary unstructured grids. *International Journal for Numerical Methods in Fluids* 2004; **44**:377–407.
6. Karimian SAM, Straatman AG. Discretization and parallel performance of an unstructured Navier–Stokes solver. *International Journal for Numerical Methods in Fluids* 2006; **52**:591–615.
7. Baserinia AR, Stubley GD. Improved Hessian reconstruction scheme for cell-centered finite volume method. *Proceedings of the 13th Annual Conference of the CFD Society of Canada*, St. John's, Newfoundland, Canada, 2005; 149–152.
8. Blazek J. *Computational Fluid Dynamics*: *Principles and Applications* (2nd edn). Elsevier: Oxford, U.K., 2005.
9. Mavriplis DJ. Revisiting the least squares procedure for gradient reconstruction on unstructured meshes. *AIAA Paper 2003-3986*, 2003.
10. Patankar SV. *Numerical Heat Transfer and Fluid Flow*. Hemisphere: New York, NY, 1980.
11. Gambit Version 2. *Gambit 2 User's Guide*. Fluent: Lebanon, NH, 2001.

DOI: 10.1002/fld